

Role of 5-aminolevulinic acid-conjugated gold nanoparticles for photodynamic therapy of cancer

Zhenxi Zhang
Sijia Wang
Hao Xu
Bo Wang
Cuiping Yao

Role of 5-aminolevulinic acid-conjugated gold nanoparticles for photodynamic therapy of cancer

Zhenxi Zhang,[†] Sijia Wang,[†] Hao Xu, Bo Wang, and Cuiping Yao*

Xi'an Jiaotong University, Institute of Biomedical Analytical Technology and Instrumentation, School of Life Science and Technology, Key Laboratory of Biomedical Information Engineering of Ministry of Education, 28 Xianning Xi Road, Xi'an, Shaanxi 710049, China

Abstract. There are three possible mechanisms for 5-aminolevulinic acid (5-ALA) conjugated gold nanoparticles (GNPs) through electrostatic bonding for photodynamic therapy (PDT) of cancer: GNPs delivery function, singlet oxygen generation (SOG) by GNPs irradiated by light, and surface resonance enhancement (SRE) of SOG. Figuring out the exact mechanism is important for further clinical treatment. 5-ALA-GNPs and human chronic myeloid leukemia K562 cells were used to study delivery function and SOG by GNPs. The SRE of SOG enabled by GNPs was explored by protoporphyrin IX (PpIX)-GNPs conjugate through electrostatic bonding. Cell experiments show that the GNPs can improve the efficiency of PDT, which is due to the vehicle effect of GNPs. PpIX-GNPs conjugate experiments demonstrated that SOG can be improved about 2.5 times over PpIX alone. The experiments and theoretical results show that the local field enhancement (LFE) via localized surface plasmon resonance (LSPR) of GNPs is the major role; the LFE was dependent on the irradiation wavelength and the GNP's size. The LFE increased with an increase of the GNP size ($2R \leq 50$ nm). However, the LSPR function of the GNPs was not found in cell experiments. Our study shows that in 5-ALA-conjugated GNPs PDT, the delivery function of GNPs is the major role. © 2015 Society of Photo-Optical Instrumentation Engineers (SPIE) [DOI: [10.1117/1.JBO.20.5.051043](https://doi.org/10.1117/1.JBO.20.5.051043)]

Keywords: local field enhancement; gold nanoparticles; quasi-static theory; conjugates of 5-ALA-GNPs; photodynamic therapy.

Paper 140689SSRR received Oct. 20, 2014; accepted for publication May 5, 2015; published online May 28, 2015.

1 Introduction

Since photodynamic therapy (PDT) has many advantages such as its minimally invasive procedure, low morbidity, minimum functional disturbance, good tolerance, ability to be used repeatedly at the same site, and the fact that it is largely an outpatient therapy,^{1,2} it is a promising treatment modality for cancers and other malignant diseases.

As of 2010, only three classes of photosensitizers (PSs) for PDT had entered clinical use for cancer therapy.³ Due to its capability to selectively induce accumulation of protoporphyrin IX (PpIX) in a multitude of different pathologies, 5-aminolevulinic acid (ALA) and its derivatives have attracted enormous attention in the field of PDT in the past two decades. The photochemical and photophysical properties of PpIX have been used for the fluorescence photo detection and photodynamic treatment of neoplasms in several medical indications, in which conversion of ALA into PpIX seems to preferentially take place. However, due to the hydrophilic properties of 5-ALA, 5-ALA-PDT may clinically be limited by the rate of ALA uptake into the neoplastic cells and/or its penetration through the tissue.⁴

Gold nanoparticle (GNP) conjugates exhibit properties unique from both their parent molecules and their particle scaffold. They can increase binding affinity and targeting selectivity when functionalized with multiple targeting groups, as well as tumor-selective uptake because of their size and the enhanced permeability and retention (EPR) effect.⁵ GNPs are also widely used in biomedical imaging and diagnostic tests

due to their special optical properties.^{6–8} Moreover, no evidence of systemic toxicity caused by the GNPs was found in animal studies,⁹ and the nanoparticle form of gold has successfully completed a Phase I clinical trial as a drug delivery agent [tumor necrosis factor (TNF) bound to GNP surface (CYT-6091)],¹⁰ especially with the recent demonstration that metallic nanoparticles can enhance singlet oxygen generation (SOG) of a PS.¹¹

Many groups found that the GNPs can enhance SOG or the photodynamic therapy efficiency of different PSs, such as phthalocyanines,^{12–17} toluidine blue O,¹⁸ indocyanine green,^{19,20} AIPcS₄,²¹ and hematoporphyrin.²² Similar to GNPs, gold nanorods (GNRs) conjugated with PS. drugs also find applications in PDT.^{17–19,21} Moreover, both *in vitro* and *in vivo* PDTs using PS-conjugated GNPs show extensive damage of cancer cells, blood capillaries, and endothelial cells.^{12,23–26} In these researches, most researchers believed that the GNPs are efficient drug delivery vectors.^{16,21,26–32} Some groups observed that the GNPs can enhance quantum yields of singlet oxygen.^{23,24} Terentyuk et al. observed dual-modality photodynamic and photothermal treatment of tumors *in vivo* with GNRs.³³ The mechanism of the gold (metal) nanoparticles enhanced SOG is of growing interest. Most of the scientists believed that this effect is due to localized surface plasmon resonance (LSPR) of the metal nanoparticles.^{11,24–27,34,35} Pasparakis speculated a possible mechanism which may involve Plasmon-mediated electron emission from the GNPs with subsequent interactions with the surrounding media which leads to SOG.³⁶ When the LSPR absorption band appears, the local electromagnetic fields

*Address all correspondence to: Cuiping Yao, E-mail: zsyycp@mail.xjtu.edu.cn

[†]These authors contributed equally to this study.

are significantly enhanced.³⁷ Therefore, enhanced electromagnetic fields in proximity to metal nanoparticles are the basis for the enhancement of the SOG. However, most of them have used extraneous PSs and have not studied whether the above three functions worked together. Additionally, few attempts have been made to model the relative increase in SOG from PSs. Zhang et al. used finite-difference time-domain calculations to simulate the electric field enhancements of a 365-nm source around a 100-nm silver nanoparticle to estimate the increase in SOG,¹¹ which is based on the extent of the net system absorption. Oo et al. applied Mie scattering theory to calculate the particle size-dependent electric field scattering and assess the enhanced SOG. They thought that the localized plasmonic field of Au NPs plays a similar role in both SOG and surface-enhanced Raman scattering enhancement.³⁵ In both models, only the metal nanoparticles were involved without taking account of the PS.

In this study, an endogenous PS was used to form 5-ALA-GNP conjugate, which was used to observe the PDT efficiency *in vitro*, and in order to find the mechanism, we measured the PpIX production and SOG in cells. The PpIX-GNP system was used to study the surface resonance enhancement. We also attempted to explain the experimental results of PpIX-GNPs by using the core-shell model and calculate the local field factor using the quasistatic theory.

2 Materials and Methods

2.1 Photodynamic Therapy System

In this study, we used different irradiation systems, including a 502-nm light-emitting diodes (LEDs) array that contains 96 LEDs corresponding to 96 well plates, 635-nm continuous wavelength semiconductor laser, and xenon lamp. We preferred to select a green LED array as irradiation light for its lower cost and the absence of pain for longer irradiation; 635-nm laser and xenon lamp were selected for comparison. The laser beam was collimated through fiber and the beam diameter was adjusted to the size of the well by optical lens. A xenon lamp can directly irradiate the 96-well plate.

2.2 5-ALA-GNP and PpIX-GNP Conjugation

5-ALA and PpIX conjugated with GNPs through electrostatic interaction between positive GNPs and negative 5-ALA and PpIX under the alkalinity environment. 5-ALA-GNPs and PpIX-GNP conjugates were prepared by mixing 500 μ l 0.1 nM cationic GNPs with 500 μ l 4 mM 5-ALA (Sigma, USA) and 2 mM PpIX (Sigma, USA) in HEPES buffer (pH 7.4, Sigma, USA) rapidly at room temperature. The cationic GNPs were synthesized by mixing poly (diallyldimethylammonium chloride) (PDDA, sigma) and HAuCl₄ (Sigma, USA), and then the mixture was heated with a microwave. In order to adjust the size of the GNPs, we used three different ratios of PDDA and HAuCl₄ for the reaction (Table 1).

The colors of the resultant GNPs and 5-ALA-GNPs conjugate were both light amarant red.^{26,38,39} The absorption spectra of GNPs and 5-ALA-GNPs were measured on a DU-640 UV-Visible (Vis) spectrophotometer (JASCO, Japan). The conjugates were confirmed by using a transmission electron microscopy (JEM-200CX, HITACHI, Japan) and a particulate size description analyzer (Mastersizer 2000, Malvern, England).

Table 1 Character of three different size gold nanoparticles (GNPs).

| GNP samples | Molar ratio of PDDA and HAuCl ₄ for reaction | Maximum Absorption Wavelength (nm) | Size (nm) | Molardecadic extinction coefficient (ϵ) at $\lambda = 450$ nm | Concentration (mol/L) |
|-------------|---|------------------------------------|-----------|--|------------------------|
| GNPs 1 | 1:2 | 524 | 16 | 2.67×10^8 | 1.48×10^{-9} |
| GNPs 2 | 1:1 | 526 | 25 | 1.10×10^9 | 3.47×10^{-10} |
| GNPs 3 | 2:1 | 530 | 33 | 2.66×10^9 | 1.31×10^{-10} |

2.3 Cell Culture and Photodynamic Therapy Treatment

Human chronic myeloid leukemia K562 was kindly provided by Zhang, (Northwest University, Xi'an, China). Cells were routinely grown in suspension culture in a Roswell Park Memorial Institute (RPMI) 1640 (1 \times) medium with HEPES and L-glutamine medium supplemented with 10% fetal calf serum and antibiotic/antimycotic solution in a 37°C humidified incubator (5% CO₂, 95% air).

Cells at logarithmic growth phase were spun down at 1400 rpm for 5 min at 20°C and then seeded in serum-free medium at a density of about 10⁶/ml in 96 well plates (100 μ l/well). 10 μ l 2 mM 5-ALA, 0.1 nM GNPs, and 2 mM 5-ALA-GNPs conjugates were added to the cell suspensions in different wells. The mixtures were incubated for 6 h in dark, during which cells can uptake 5-ALA, GNPs, conjugates and the uptaken 5-ALA can generate PpIX in cells, then the well plates were carefully washed twice with phosphate-buffered saline (PBS) and then refreshed with 100 μ l serum-free medium for each well. For the PDT-treated group, the mixture of cells and reagent was irradiated with three different light sources with different times. The light sources included 502-nm LED (5 mW/cm², irradiation for 1 h), 635-nm continuous wavelength laser (40 mW/cm², irradiation for 10 min), and xenon lamp (40 mW/cm², irradiation for 10 min).

After irradiation, the cell suspension was washed twice with PBS to remove free drugs and refreshed with 100 μ l medium containing 10 μ l of cell counting kit-8. Cell viability was valued by the absorption of each well at 450 nm with an MK3 96-well microplate reader (Labsystems, Finland).

2.4 PpIX and Singlet Oxygen Generation Test

To quantificate the internalized amount of 5-ALA in K562 cells treated with 5-ALA and 5-ALA-GNPs, we detected the PpIX generation in cells after the incubation and SOG after irradiation. Briefly, the K562 cell suspensions at a density of 10⁶/ml were seeded in six well plates (2 ml/well). Then cells were incubated with 200 μ l 2 mM 5-ALA, 0.1 nM GNPs, and 2 mM 5-ALA-GNPs for 6 h under dark conditions.³⁹ The samples were centrifuged at 12,000 g for 5 min, washed with PBS twice to remove the remaining materials, and resuspended in sodium dodecyl sulfate lysis buffer. The samples were then incubated for 20 min on ice and centrifuged at 12,000 g for 5 min. The suspension solutions of these centrifuged samples were collected and divided into two parts. One part of the collection was sent to a spectrometer (F-4500, Hitachi, Japan) to measure the PpIX fluorescence intensity (excitation wavelength: 410 nm).

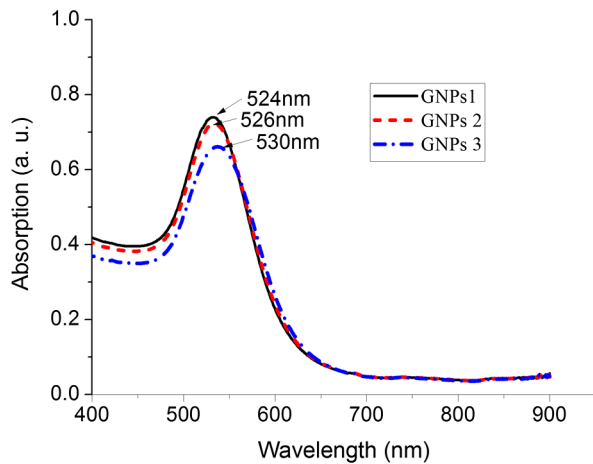


Fig. 1 Absorption spectra of three different sized gold nanoparticles (GNPs).

Another part was mixed with singlet oxygen sensor green reagent (SOSGR) and irradiated with different light sources for different times as mentioned in Sec. 2.3.

For comparison, we also directly detected singlet oxygen of different size GNPs and PpIX conjugates after light irradiation as Xu et al used.³⁹ Briefly, 2 ml 1 mM PpIX solution, three different GNPs–PpIX conjugates prepared from 1 mM PpIX mixed with 0.1 nM 16, 25, and 33 nm-sized GNPs, and control solution containing only ultrapure water (ventilated with nitrogen to eliminate oxygen) were mixed with 20 μ l SOSGR, respectively.

The mixed solutions were plated into a 6-well plate and irradiated with different light sources for different times as mentioned in Sec. 2.3. The amounts of singlet oxygen generated from both (in cells treated with 5-ALA and direct irradiation of PpIX) were detected by the fluorescence intensity of the SOSGR using a fluorospectrometer (F-4500, Hitachi, Japan).

3 Results

3.1 Characterization of GNPs and PS-GNPs Conjugation Confirmation

GNPs with three different sizes were prepared and used in our study (Table 1). Figure 1 showed the absorption spectrum of these three GNPs. The size of GNPs showed in Table 1 was measured by Malvern particulate size description analyzer and the concentration of GNPs was estimated by the molar decadic extinction coefficient at 450 nm of GNPs according to the data published by Haiss et al.⁴⁰

The maximum of the surface plasmon resonance (SPR) absorption of gold colloids is known to red shift with increasing particle diameter.⁴¹ Our study found that the size of PS–GNPs conjugates is slightly bigger than pure GNPs.⁴² As showed in Figs. 2(c) and 2(d), the SPR absorption peaks appeared at about 524, 526, and 540 nm for GNPs, 5-ALA–GNPs conjugates and PpIX–GNPs, respectively. The electron microscopy images [Figs. 2(a) and 2(b)] also slightly showed the size increase of the GNPs after conjugating with ALA from 16 to 18 nm.

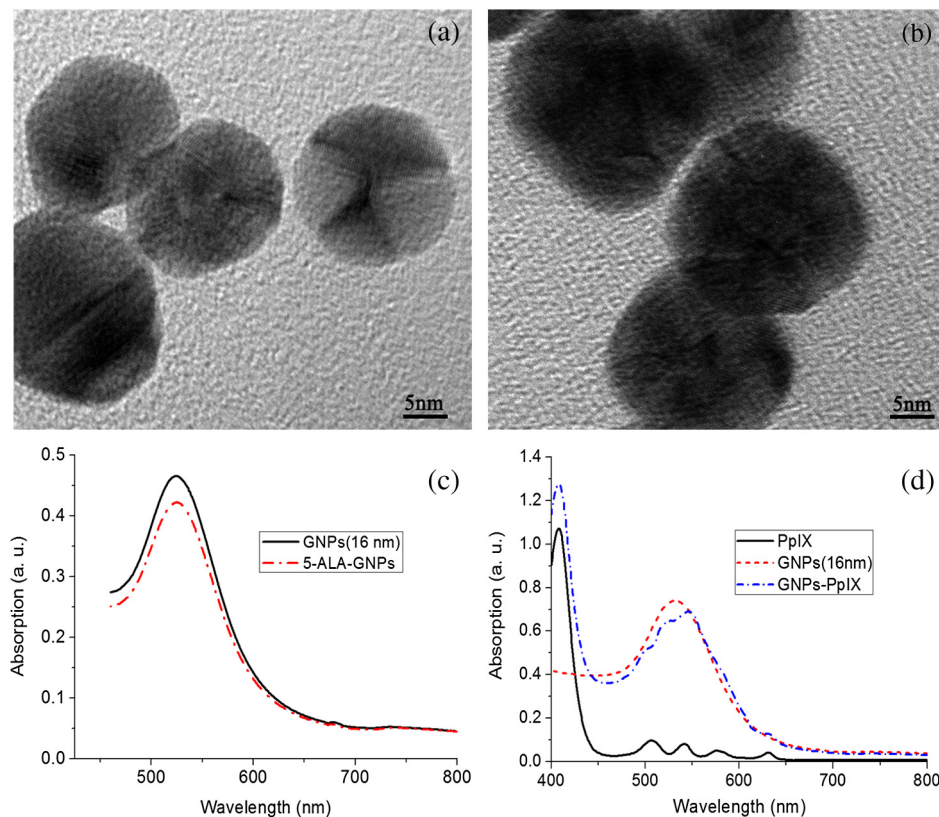


Fig. 2 The electron microscopy images of 16 nm GNPs (a) and 5-ALA-GNPs; (b) meanwhile, the absorption spectra of GNPs and 5-ALA-GNPs conjugate, GNPs, (c) protoporphyrin IX (PpIX) and GNPs–PpIX (d) were given.

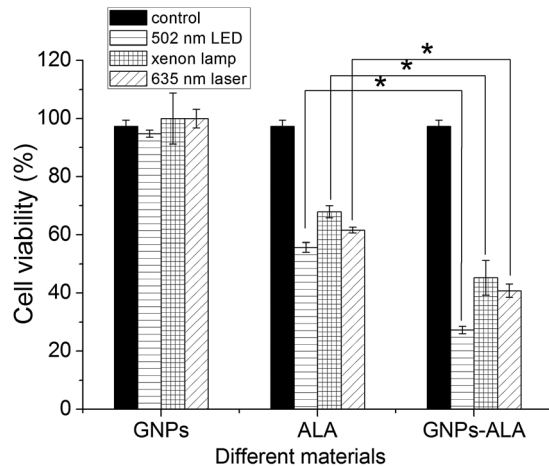


Fig. 3 Cell viability after treatment with GNPs, 5-ALA and 5-ALA-GNPs and irradiated by different light sources. Asterisk indicates statistically significant difference in cell viability between samples after *t* test analysis ($p < 0.05$).

3.2 Cell Experiments for Photodynamic Therapy Treatment

As a precursor of PS, 5-ALA was finally transferred into PpIX in cells that subsequently accumulate in cancer cells. PpIX has several absorption wavelength peaks [Fig. 2(d)]; in clinical PDT, normally a 635-nm wavelength was used for its deeper penetration. In our study, K562 cells treated with GNPs, 5-ALA, and 5-ALA-GNP were irradiated with different light sources and for different times. The results of cell viability according to the fluorescence of kit-8 are shown in Fig. 3. Samples treated with 5-ALA-GNP conjugates exhibited superior cell killing efficiency compared with those treated with 5-ALA only, while samples treated with GNPs only showed nearly no damage to the cells. Since the LEDs array has power density of 5 mW/cm² that has no effect on humans for a long time (that is people can endure the irradiation for a long time), we irradiate the cells with an LED array for 1 h. For the other two light sources, cells were irradiated for 10 min with a power density of 40 mW/cm². Therefore, for each light source, the irradiation dose was equal (24 J/cm²). Among these three light sources, samples treated with the 502-nm LED array irradiation showed better cell killing efficiency.⁴³

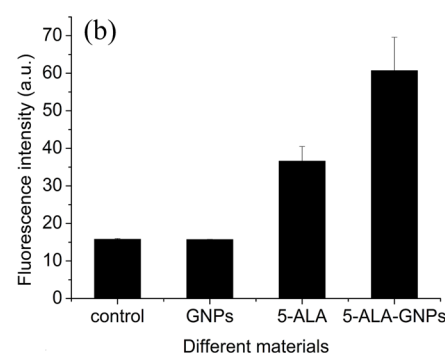
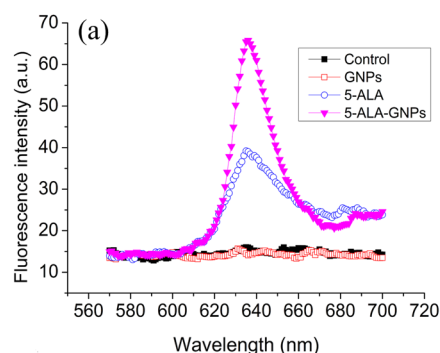


Fig. 4 PpIX fluorescence intensity detection from cell lysates after incubation with GNPs, 5-ALA and 5-ALA-GNPs for 6 h: (a) the fluorescence spectra and (b) the fluorescence intensity at 635-nm wavelength.

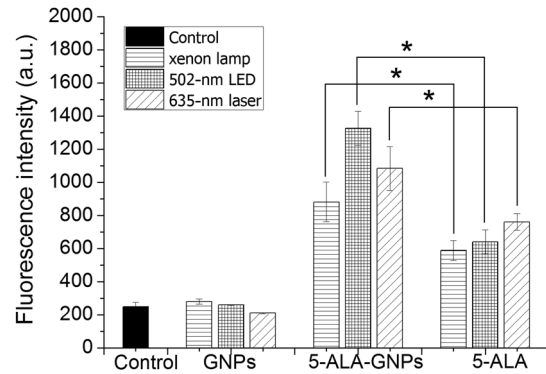


Fig. 5 Singlet oxygen sensor green reagent (SOSGR) fluorescence intensity of 5-ALA-GNPs, 5-ALA, and GNPs alone from cell lysates after irradiation. Asterisk indicates statistically significant difference in cell viability between samples after *t* test analysis ($p < 0.05$).

3.3 PpIX and Singlet Oxygen Generation

For detection of PpIX that was generated by 5-ALA in cancer cells, the 410-nm excitation wavelength is used, and the emission fluorescence peak is at about 635 nm. Figure 4 shows the PpIX fluorescence intensity from the lysates of cells incubated with GNPs, 5-ALA, and 5-ALA-GNPs for 6 h. The results showed that the 5-ALA-GNPs-treated cells yielded about two times PpIX than that of 5-ALA alone. GNPs-treated cell lysates contained almost no PpIX compared to the result of the control samples, which were nontreated cell lysates.

The generation of the singlet oxygen is an important indicator of cell killing efficiency in PDT. Although several singlet oxygen detection reagents are available, our choice of singlet oxygen sensor green reagent depends on the fact that it is highly selective for singlet oxygen. SOSGR has a green fluorescence emission peak at 525 nm. The fluorescence intensity treated cells can be used to estimate the SOG, and the results measured from cell lysates are shown in Fig. 5. The results indicate that with different light irradiation, cells treated with 5-ALA-GNPs all produce more singlet oxygen than those treated with 5-ALA alone, and the cells incubated with GNPs alone nearly produce no singlet oxygen compared with the control (nontreated cells). However, the improvement of SOG is different according to different light irradiation. Green LED irradiation gives a greater improvement efficiency, whereas the SOG is about 2.74 times higher for conjugates than those of the PpIX alone. For xenon lamp and 635-nm laser irradiation, the SOG improvement is about 1.7 times.

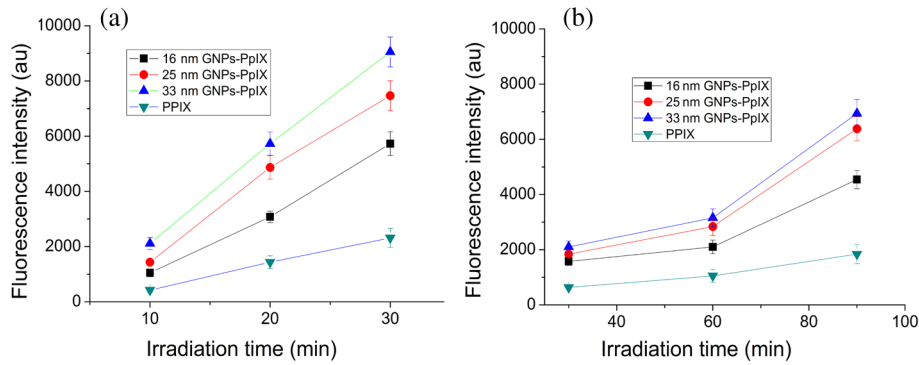


Fig. 6 Size and irradiation time-dependent singlet oxygen generation (SOG) of PpIX-GNPs conjugates, PpIX and GNPs alone with different light irradiations: (a) 635-nm laser (40 mW/cm^2) and (b) 502-nm LED (5 mW/cm^2).

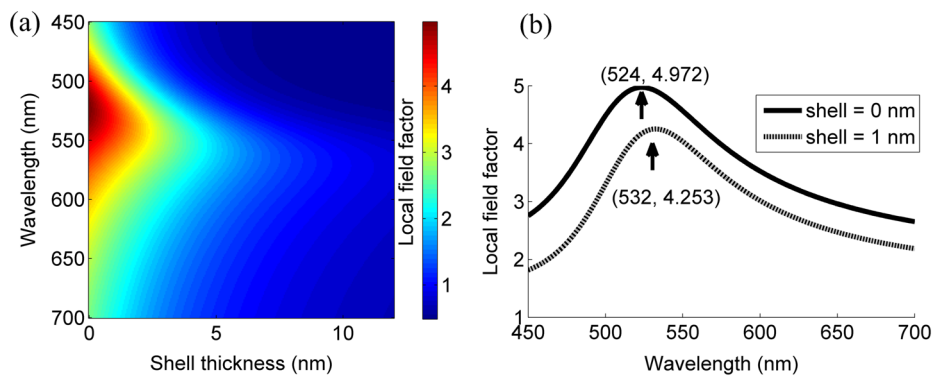


Fig. 7 (a) Quasistatic calculations of the local electric field factor versus shell thickness at different wavelengths. (b) Local field factor as a function of wavelength at a fixed shell thickness.

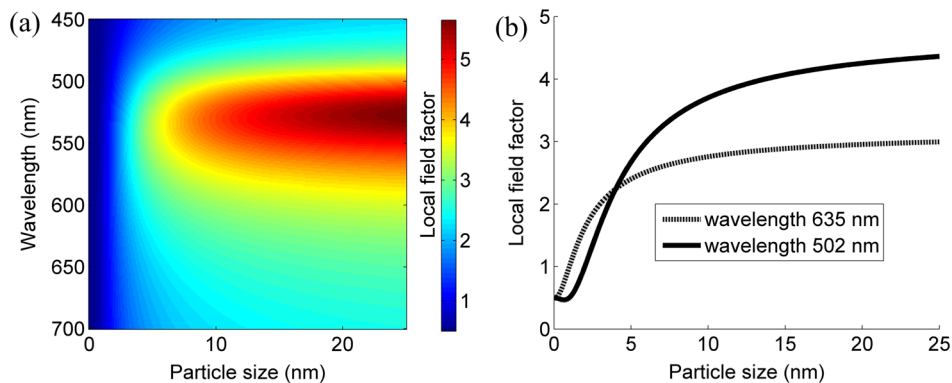


Fig. 8 (a) Quasistatic calculations of the local electric field factor versus GNP size at different wavelengths. (b) Local field factor as a function of GNP size at a fixed wavelength.

PpIX and three different PpIX-GNPs conjugates were directly irradiated with two lights. The results of SOG (Fig. 6) are similar to that in cells with 5-ALA (Fig. 5), PpIX-GNPs conjugates generated more singlet oxygen than PpIX alone. However, the improvement of SOG of PpIX-GNPs to PpIX is much greater than 5-ALA-GNPs to 5-ALA in cells. In addition, the fluorescence intensity of SOSGR increased with the increase of GNP size and irradiation time.

4 Discussion and Conclusion

Figure 3 shows that 5-ALA-GNP conjugates exhibited superior cell killing efficiency compared with 5-ALA alone. Several studies also demonstrated that 5-ALA *in vitro* PDT efficiency can be improved by GNPs,^{27,39} and GNPs can deliver much more 5-ALA into cells. PpIX measurement and SOG detection can be used to discover part of the mechanism of this process. In our study, Fig. 4 shows that 5-ALA-GNPs conjugates generated

double the amount of PpIX than 5-ALA alone in K562 cells, which confirmed the GNPs delivery function because PpIX was transformed from ALA in the cells. After uptake by the cells, 5-ALA-GNPs conjugates were exposed in intracellular acidic environments. 5-ALA changed to be positively charged, separated from the surface of GNPs and was transferred into PpIX by cells. Therefore, more PpIX generation of 5-ALA-GNPs in cells indicates more internalized 5-ALA; meanwhile, the result explained the improved SOG by 5-ALA-GNPs is shown in Fig. 5. The results demonstrated that the enhancement of SOG is smaller than the improvement of PpIX except for the green LED arrays. This means the SOG came directly from PpIX except for the green LED arrays. Therefore, we proved that the improved tumor cell-killing efficiency of 5-ALA-GNPs was mainly due to the fact that GNPs can deliver more 5-ALA into cells.

However, the improved SOG phenomena found in PpIX-GNPs systems, as Fig. 6 showed, cannot be explained with the same reason. In this study, PpIX-GNPs and PpIX were directly irradiated in HEPES buffer and did not involve the cell uptake. PpIX attaches to the GNPs surface through electrostatic interaction since its electronegativity in HEPES buffer (pH 7.2) during the irradiation. Vankayala et al and Jiang et al. showed that GNP itself can effectively generate singlet oxygen induced by light,^{44,45} but in these papers, GNPs were usually induced by a UV light with a large irradiation power (around 100 W) and the generation of singlet oxygen was mainly the result of two-photon excitation instead of the mW level irradiation power with 502 and 635 nm wavelengths in our study. Maybe this is the reason why the GNP itself hardly generates singlet oxygen in our experiment (Fig. 5). In addition, Fig. 6 also shows the SOG of PpIX-GNPs conjugates increased with the increase of GNP size for both light sources. Therefore, we demonstrate that, in this case, the enhanced SOG of PpIX-GNPs is due to the local field enhancement effect of GNPs.

To analyze this mechanism of the gold-enhanced SOG, PpIX-GNPs can be considered as the core-shell structure as a model and we can use local electric field enhancement theoretical calculations to simulate the process.

For the PS-capped metal nanoparticle, the spectra are not simple super positions of the surface plasmon spectra of the metal and the absorption spectra of the PSs. The optical spectra of these PS-nanoparticle composites exhibit interferences between the molecule and the SPRs. Generally, these spectra are explained by treating the SP-nanoparticle system as a construction composed of a metal core and a PS shell having different dielectric functions, and classical electrodynamics can be used to calculate the optical properties.⁴⁶⁻⁵⁰ Zhu et al. used the core-shell model to explain the fluorescence modification of RB modulated with GNPs and demonstrated that the theoretical calculations satisfied the experimental results.⁵¹ Therefore, in this study, we speculated that the core-shell model could be used to explain the enhanced SOG of GNPs-PpIX.

In PDT, the generation of the singlet oxygen from PSs can be described as follows under the condition of sufficient oxygen

$$S^* = P^* \varphi = \varphi k I P t, \quad (1)$$

where S^* represents the SOG, P^* denotes the excited PS, η denotes the conversion rate from P to P^* , φ signifies the quantum yield of the singlet oxygen, k describes the cross section of PS at the wavelength of irradiation, P is the concentration of the PS, and I and t signify the irradiation intensity and irradiation

time, respectively. In Eq. (1), for a certain PS, η , s , φ , and k are fixed. Thus, SOG is proportional to PS concentration, irradiation intensity, and time. In this study, the PS concentration and irradiation time for all samples were the same; we assumed that the irradiation intensity for the sample including GNPs could be changed by local field enhancement. Therefore, we attempted to explain the experimental results of the GNP-enhanced single oxygen generation of PpIX by using this core-shell model to calculate the local field factor R , thus the irradiation intensity for Au-PpIX could be given by

$$I_{\text{Au-PpIX}} = I_{\text{PpIX}} R, \quad (2)$$

where $I_{\text{Au-PpIX}}$ denotes the irradiation intensity to GNPs-PpIX, I_{PpIX} signifies the irradiation intensity to pure PpIX, and R denotes the local field factor of PpIX-coated GNPs.

We calculated the size-dependent and shell thickness-dependent local field factor R in the wavelength range of 450 and 700 nm. The corresponding results are shown in Figs. 7 and 8.

Figure 7(a) shows the quasistatic calculation of the local field factor at different wavelengths versus radial distance with a gold core diameter of 16 nm. For a fixed wavelength, the local field factor decreased with the increase of the shell thickness. For a fixed thickness, the local field factor was a function of the wavelength, and for every certain wavelength, a maximum value of R existed, and the wavelength was close to the SPR band of the nanoshell. In this study, the shell thickness was 1 nm. According to the calculations, local field factors were about 3.392 and 2.624 for the irradiation wavelength 502 nm (green LED) and 635 nm (continue wavelength laser), respectively. These findings satisfied our experimental results because of the absence of a linear relationship between the green fluorescence intensity and the SOG.⁵² Figure 7(b) shows the local field factor as a function of wavelength at a fixed shell of 0 and 1 nm. The peak was very similar to and even equal to the absorption peak as shown in Fig. 1. The increase of the wavelength resulted in the initial increase of the local field factor and then a decrease; the peak wavelength red shifted with increasing shell thickness.

In biomedical applications, the size of GNPs is an important factor because it determines its physical and chemical properties. Therefore, the electric field enhancement is affected by the GNP size. The core-shell model used to investigate the GNP size dependence of the SOG of GNP-PpIX conjugate was useful for further experiments. Figure 8(a) shows the quasistatic calculation of the local field factor at different wavelengths versus GNP size and the PS shell thickness was 1 nm. Figure 8(b) shows the local field factor as a function of GNP size at a fixed wavelength (the 502 and 635 nm we have used). The increase in GNP size resulted in the increase of the local field factor in intrinsic size regime ($2R \leq 50$ nm), for which the quasistatic approach can be used.⁵² On the other hand, because GNPs with a size of 40 to 60 nm have the best cellular uptake efficiency,⁵³⁻⁵⁶ the highest cell killing efficiency could be reached by using 40 to 60 nm GNPs as a delivery agent for 5-ALA in PDT, which has been demonstrated by Oo et al.³⁵

If the higher efficiency of 5-ALA-GNPs conjugates-based PDT was due to the GNPs delivery function and local field enhancement, the enhancement of SOG in cells should be the product of 2 (improvement of PpIX generation) and 2.5 (enhancement of SOG), which was not in accordance with experimental results. When GNPs separated from 5-ALA, 5-ALA transferred into PpIX mainly in mitochondria, while the

distribution of GNPs is not clear. Maybe that was the reason that local field enhancement of GNPs did not work in cells for 5-ALA-GNPs PDT.

In this study, the 5-ALA-GNPs conjugates were used for K562 cell destruction PDT, which induced higher tumor cell-killing efficiency compared with the 5-ALA PDT. Biocompatible GNP can be used as a promising vehicle for effective delivery of 5-ALA.²⁷ Furthermore, we observed that 5-ALA-GNPs in cells exhibited distinct single oxygen generation enhancement and different light sources resulted in different efficiencies. We model the PpIX-GNPs conjugates as a core-shell nanostructure to explain the observed single oxygen generation characters in terms of the coupling of incident light to PpIX with local field enhancement from GNPs. Calculations based on quasistatic theory indicated that the local field enhancement was different for different wavelengths. When the incident light was closed to the SPR band of the nanocore, the single oxygen generation could be effectively enhanced. Therefore, the 502-nm LED array led to higher oxygen generation than the 398 and 621 nm LED arrays.²⁷ Furthermore, the calculation and experiments both demonstrated that the GNP size was an important factor for field enhancement; SOG increased with the increase of the GNP size. However, for 5-ALA-GNPs conjugate-based PDT, the efficiency or the cell killing was mainly due to the GNPs delivery function instead local field enhancement and the SOG of the GNPs themselves.

Acknowledgments

This study was supported by the National Nature Science Foundation of China (Grant Nos. 61120106013 and 11274249) and the Fundamental Research Funds for the Central Universities (Grant No. xjj2012133).

References

- D. K. Chatterjee and Z. Yong, "Upconverting nanoparticles as nano-transducers for photodynamic therapy in cancer cells," *Nanomedicine* **3**(1), 73–82 (2008).
- J. H. Hodak, A. Henglein, and G. V. Hartland, "Photophysics of nanometer sized metal particles: electron-phonon coupling and coherent excitation of breathing vibrational modes," *J. Phys. Chem. B* **104**(43), 9954–9965 (2000).
- R. R. Allison, V. S. Bagnato, and C. H. Sibata, "Future of oncologic photodynamic therapy," *Future Oncol.* **6**(6), 929–940 (2010).
- F. Cairnduff et al., "Superficial photodynamic therapy with topical 5-aminolevulinic acid for superficial primary and secondary skin-cancer," *Brit J. Cancer* **69**(3), 605–608 (1994).
- J. A. Barreto et al., "Nanomaterials: applications in cancer imaging and therapy," *Adv. Mater.* **23**(12), H18–40 (2011).
- C. P. Yao, Z. X. Zhang, and B. L. Yao, "Laser irradiation cell photothermal therapy assisted by gold nanoparticles," *Prog. Biochem. Biophys.* **34**(3), 312–316 (2007).
- M. V. Yigit and Z. Medarova, "In vivo and ex vivo applications of gold nanoparticles for biomedical SERS imaging," *Am. J. Nucl. Med. Mol. Imaging* **2**(2), 232–241 (2012).
- C. P. Yao, X. C. Qu, and Z. X. Zhang, "Laser-based transfection method with conjugated gold nanoparticles," *Chin. Opt. Lett.* **7**(10), 898–900 (2009).
- Z. Qin and J. C. Bischof, "Thermophysical and biological responses of gold nanoparticle laser heating," *Chem. Soc. Rev.* **41**(3), 1191–1217 (2012).
- S. K. Libutti et al., "Phase I and pharma-cokinetic studies of CYT-6091, a novel PEGylated colloidal gold-rhTNF nano- medicine," *Clin. Cancer Res.* **16**(24), 6139–6149 (2010).
- Y. Zhang et al., "Plasmonic engineering of singlet oxygen generation," *Proc. Natl. Acad. Sci.* **105**(6), 1798–1802 (2008).
- M. Camerin et al., "The in vivo efficacy of phthalocyanine-nanoparticle conjugates for the photodynamic therapy of amelanotic melanoma," *Eur. J. Cancer* **46**(10), 1910–1918 (2010).
- D. C. Hone et al., "Generation of cytotoxic singlet oxygen via phthalocyanine-stabilized gold nanoparticles: a potential delivery vehicle for photodynamic therapy," *Langmuir* **18**(8), 2985–2987 (2002).
- M. E. Wieder et al., "Intracellular photodynamic therapy with photosensitizer-nanoparticle conjugates: cancer therapy using a 'Trojan horse,'" *Photochem. Photobiol. Sci.* **5**(8), 727–734 (2006).
- T. Stuchinskaya et al., "Targeted photodynamic therapy of breast cancer cells using antibody-phthalocyanine-gold nanoparticle conjugates," *Photochem. Photobiol. Sci.* **10**(5), 822–831 (2011).
- Y. Cheng et al., "Highly efficient drug delivery with gold nanoparticle vectors for in vivo photodynamic therapy of cancer," *J. Am. Chem. Soc.* **130**(32), 10643–10647 (2008).
- W. S. Kuo et al., "Gold nanorods in photodynamic therapy, as hyperthermia agents, and in near-infrared optical imaging," *Angew. Chem. Int. Edit.* **49**(15), 2711–2715 (2010).
- W. S. Kuo et al., "Antimicrobial gold nanorods with dual-modality photodynamic inactivation and hyperthermia," *Chem. Commun.* **8**(32), 4853–4855 (2009).
- L. Li et al., "Plasmonic gold nanorods can carry sulfonated aluminum phthalocyanine to improve photodynamic detection and therapy of cancers," *J. Phys. Chem. B* **114**(51), 17194–17200 (2010).
- E. S. Tuchina et al., "Phototoxic effect of conjugates of plasmon-resonance nanoparticles with indocyanine green dye on *Staphylococcus aureus* induced by IR laser radiation," *Quantum Electron.* **41**(4), 354–359 (2011).
- B. Jang et al., "Gold nanorod-photosensitizer complex for near-infrared fluorescence imaging and photodynamic/photothermal therapy in vivo," *Acs Nano* **5**(2), 1086–1094 (2011).
- B. N. Khlebtsov et al., "Enhanced photoinactivation of *Staphylococcus aureus* with nanocomposites containing plasmonic particles and hematoporphyrin," *J. Biophoton.* **6**(4), 338–351 (2013).
- L. Zhou et al., "External heavy-atomic construction of photosensitizer nanoparticles for enhanced in vitro photodynamic therapy of cancer," *J. Phys. Chem. B* **116**(42), 12744–12749 (2012).
- B. Bauer et al., "Metal nanoparticles amplify photodynamic effect on skin cells in vitro," *Proc. SPIE* **7897**, 789712 (2011).
- F. Geng et al., "Pegylated glucose gold nanoparticles for improved in-vivo bio-distribution and enhanced radiotherapy on cervical cancer," *J. Biomed. Nanotechnol.* **10**(7), 1205–1216 (2014).
- B. Wang et al., "Rose-bengal-conjugated gold nanorods for in vivo photodynamic and photothermal oral cancer therapies," *Biomaterials* **35**(6), 1954–1966 (2014).
- M. K. Oo et al., "5-aminolevulinic acid-conjugated gold nanoparticles for photodynamic therapy of cancer," *Nanomedicine* **3**(6), 777–786 (2008).
- D. Bechet et al., "Nanoparticles as vehicles for delivery of photodynamic therapy agents," *Trends Biotechnol.* **26**(11), 612–621 (2008).
- Y. Cheng et al., "Deep penetration of a PDT drug into tumors by non-covalent drug-gold nanoparticle conjugates," *J. Am. Chem. Soc.* **133**(8), 2583–2591 (2011).
- W.-S. Kuo et al., "Gold nanomaterials conjugated with indocyanine green for dual-modality photodynamic and photothermal therapy," *Biomaterials* **33**(11), 3270–3278 (2012).
- N. F. Gamaleia et al., "Photodynamic activity of hematoporphyrin conjugates with gold nanoparticles: experiments in vitro," *Exp. Oncol.* **32**(1), 44–47 (2010).
- B. Jang and Y. Choi, "Photosensitizer-conjugated gold nanorods for enzyme-activatable fluorescence imaging and photodynamic therapy," *Theranostics* **2**(2), 190–197 (2012).
- G. Terentyuk et al., "Gold nanorods with a hematoporphyrin-loaded silica shell for dual-modality photodynamic and photothermal treatment of tumors in vivo," *Nano Res.* **7**(3), 325–337 (2014).
- S. M. Mooi and B. Heyne, "Amplified production of singlet oxygen in aqueous solution using metal enhancement effects," *Photochem. Photobiol.* **90**(1), 85–91 (2014).
- M. K. Oo et al., "Gold nanoparticle-enhanced and size-dependent generation of reactive oxygen species from protoporphyrin ix," *ACS Nano* **6**(3), 1939–1947 (2012).
- G. Pasparakis, "Light-induced generation of singlet oxygen by naked gold nanoparticles and its implications to cancer cell phototherapy," *Small* **9**(24), 4130–4134 (2013).

37. P. Bharadwaj, A. Bouhelier, and L. Novotny, "Electrical excitation of surface plasmons," *Phys. Rev. Lett.* **106**(22), 226802 (2011).
 38. X. Qu et al., "Anti-CD30-targeted gold nanoparticles for photothermal therapy of L-428 Hodgkin's cell," *Int. J. Nanomed.* **7**, 6095–6103 (2012).
 39. H. Xu et al., "Effects of light irradiation upon photodynamic therapy based on 5-aminolevulinic acid-gold nanoparticle conjugates in K562 cells via singlet oxygen generation," *Int. J. Nanomed.* **7**, 5029–5038 (2012).
 40. W. Haiss et al., "Determination of size and concentration of gold nanoparticles from UV-Vis spectra," *Anal. Chem.* **79**(11), 4215–4221 (2007).
 41. S. Link and M. A. El-Sayed, "Size and temperature dependence of the plasmon absorption of colloidal gold nanoparticles," *J. Phys. Chem. B* **103**(21), 4212–4217 (1999).
 42. C. P. Yao et al., "New photosensitizer 5-ALA-GNPs for photodynamic therapy and its spectral analysis," *Spectrosc. Spectral Anal.* **32**(9), 2519–2522 (2012).
 43. R. Steiner, "laser-tissue interactions," in *Laser and IPL Technology in Dermatology and Aesthetic Medicine*, S. K. Christian Raulin, Ed., pp. 23–36, Springer, Berlin, Herdelberg (2011).
 44. R. Vankayala et al., "Metal nanoparticles sensitize the formation of singlet oxygen," *Angew. Chem. Int. Ed.* **50**(45), 10640–10644 (2011).
 45. C. Jiang et al., "Two-photon induced photoluminescence and singlet oxygen generation from aggregated gold nanoparticles," *ACS Appl. Mater. Interfaces* **5**(11), 4972–4977 (2013).
 46. C. Flors et al., "Imaging the production of singlet oxygen in vivo using a new fluorescent sensor, singlet oxygen sensor green (R)," *J. Exp. Botany* **57**(8), 1725–1734 (2006).
 47. G. P. Wiederrecht, G. A. Wurtz, and J. Hranisavljevic, "Coherent coupling of molecular excitons to electronic polarizations of noble metal nanoparticles," *Nano Lett.* **4**(11), 2121–2125 (2004).
 48. A. M. Kelley, "A molecular spectroscopic description of optical spectra of j-aggregated dyes on gold nanoparticles," *Nano Lett.* **7**(10), 3235–3240 (2007).
 49. T. Uwada et al., "Single particle spectroscopic investigation on the interaction between exciton transition of cyanine dye j-aggregates and localized surface plasmon polarization of gold nanoparticles," *J. Phys. Chem. Lett. C* **111**(4), 1549–1552 (2007).
 50. J. Zhu, "Spatial dependence of the local field enhancement in dielectric shell coated silver nanospheres," *Appl. Surf. Sci.* **253**(21), 8729–8733 (2007).
 51. J. Zhu, K. Zhu, and L.-Q. Huang, "Using gold colloid nanoparticles to modulate the surface enhanced fluorescence of rhodamine B," *Phys. Lett. A* **372**(18), 3283–3288 (2008).
 52. H. Lin et al., "Feasibility study on quantitative measurements of singlet oxygen generation using singlet oxygen sensor green," *J. Fluoresc.* **23**(1), 41–47 (2013).
 53. W. Jiang et al., "Nanoparticle-mediated cellular response is size-dependent," *Nat. Nanotechnol.* **3**(3), 145–150 (2008).
 54. D. A. Giljohann et al., "Oligonucleotide loading determines cellular uptake of DNA-modified gold nanoparticles," *Nano Lett.* **7**(12), 3818–3821 (2007).
 55. B. Chithrani and W. Chan, "Elucidating the mechanism of cellular uptake and removal of protein-coated gold nanoparticles of different sizes and shapes," *Nano Lett.* **7**(6), 1542–1550 (2007).
 56. S.-H. Wang et al., "Size-dependent endocytosis of gold nanoparticles studied by three-dimensional mapping of plasmonic scattering images," *J. Nanobiotechnol.* **8**(1), 33–43 (2010).
- Zhenxi Zhang** received his PhD in biomedical engineering from Xi'an Jiaotong University in 1990. He has been to Germany many times as a researcher, including the University of Stuttgart, the GSF-National Research Center for Environment and Health, Huboldt University, Wilhelmshaven University of Applied Sciences, Lübeck University of Applied Sciences, Lübeck University, and so on. His research focuses on the applied technology in biomedical optics, optical biophysics, biomedical optical imaging process, and spectral analysis method.
- Sijia Wang** is a PhD student in biomedical engineering at Xi'an Jiaotong University, China. He received his master's degree in biomedical engineering in 2012. He works on the research of biomedical optics including biomedical application of gold nanoparticles (GNPs) and photodynamic therapy.
- Hao Xu** is a PhD student in Xi'an Jiaotong University, China. He received his BS and MS degrees in biotechnology and biophysics in 2007 and 2010. He was a joint PhD student and research associate at the Wellman Center for Photomedicine, Harvard Medical School, Massachusetts, in 2012. He is interested in developing new photodynamic treatments using nanotechnology. His research focuses on exploring new photodynamic therapy methods with conjugating different photosensitizers with metal nanoparticles and nanoliposomes.
- Bo Wang** received his BS degree in biomedical engineering from Xi'an Jiaotong University, Xi'an, China, in 2007, and his MS degree in biomedical engineering from Xi'an Jiaotong University in 2009. Currently, he is working toward his PhD at Xi'an Jiaotong University. His research interests include image processing and medical imaging.
- Cuiping Yao** received her BS degree in electronic engineering from Shenyang Aerospace University and her MS and PhD degrees in biomedical engineering from Xi'an Jiaotong University in 2006. Later she joined Xi'an Jiaotong University. Her research focuses on the photothermal heating and photodynamic therapy of gold nanoparticles for diagnosis and treatment of disease including cancer.